Supplementary Information

Confining Acetonitrile-I_2 Complexes via Fe Single-Atom Sites for Rapid and Reversible Iodine Redox Kinetics at −40°C

Chuanyang Li,[†,a] Chengxu Niu,[†,a] Ruoyang Xu,[b] Jikun Li,[a] Yanchen Liu,[a] Hengjian Pu,[a] Jin Li,[a] Teng Zhai,*[a] and Hui Xia[a]

[a]School of Materials Science and Engineering, Nanjing University of Science and Technology, Nanjing 210094, China

[b]College of Science, Mathematics and Technology, Wenzhou-Kean University, Wenzhou 325060, China

E-mail: tengzhai@njust.edu.cn

Experimental section

Synthesis of Fe-PC/I_2 and PC/I_2

Porous carbon (0.15 g) was dispersed in 30 mL of 0.05 M $Fe(NO_3)_3$ solution and incubated at 40 °C for 12 h. The resulting mixture was centrifuged at 9000 rpm for 5 min per cycle, and the process was repeated three times. The collected precipitate was dried at 80 °C for 24 h, followed by annealing at 800 °C for 2 h under an Ar/H_2 atmosphere with a heating rate of 5 °C min^{-1}. The resulting powder was then immersed in concentrated hydrochloric acid (HCl) at 60 °C for 8 h, washed thoroughly with deionized water, and dried to obtain Fe-PC. Fe-PC/I_2 and PC/I_2 cathodes were prepared by mixing iodine with the respective carbon hosts at a mass ratio of 1:1, followed by thermal treatment at 120 °C for 24 h. For electrode fabrication, the Fe-PC/I_2 or PC/I_2 composite was combined with Ketjen black and PTFE in isopropanol at a weight ratio of 8:1:1 to obtain a homogeneous slurry. This slurry was spread onto a glass plate and dried at 70 °C for 8 h. The iodine loading of the resulting electrode was controlled between 1 and 1.5 mg cm^{-2}.

Electrochemical measurements

To evaluate the electrochemical performance of the Fe-PC/I_2 and PC/I_2 electrodes, CR2025-type coin cells were assembled. The Fe-PC/I_2 or PC/I_2 composite was used as the cathode, while metallic zinc foil served as the anode. Whatman GF/D membrane was employed as the separator. The electrolyte consisted of 1 M $Zn(ClO_4)_2$ in acetonitrile (ACN). Galvanostatic charge-discharge (GCD) tests were conducted on Neware BTS-610 battery testing system within a voltage window of 0.6~1.6 V versus Zn^{2+}/Zn at various current densities. Cyclic voltammetry (CV) and electrochemical impedance spectroscopy (EIS) measurements were carried out on a Corrtest CS2350H electrochemical workstation.

Material characterization

X-ray diffraction (XRD) patterns were collected on a Bruker D2 Advance diffractometer using Cu Kα radiation (λ = 1.5418 Å) with a scanning speed of 2° min^{-1} over a 2θ range of 10°−80°. Scanning electron microscopy (SEM) images were obtained using a JEOL JSM-7500F field-emission scanning electron microscope. UV-vis absorption spectra were collected using a Shimadzu UV-3600i Plus UV-Vis-NIR spectrophotometer. Raman spectroscopies were collected using a portable Raman spectrometer (i-Raman Prime 532H, Metrohm) over the range of 100–500 cm^{-1}. For in situ Raman spectroscopies at 25 °C, spectra were directly acquired from the electrode in an operating coin cell equipped with a quartz optical window, without disassembling the cell. For ex situ Raman measurements at −40 °C, the electrodes were extracted from disassembled cells, rinsed with anhydrous acetonitrile to remove residual electrolyte, and dried under vacuum prior to analysis. Differential scanning calorimetry (DSC) was performed on a TGA/DSC3+ system (METTLER Toledo). Approximately 5-10 mg of electrolyte was sealed in an aluminum crucible. The measurement was conducted under nitrogen atmosphere from 25 °C to −80 °C at a rate of 5 °C min^{-1}.

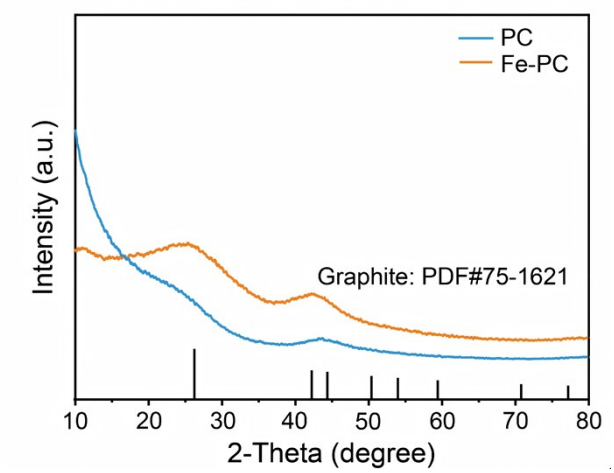

Figure S1. XRD patterns of PC and Fe-PC samples.

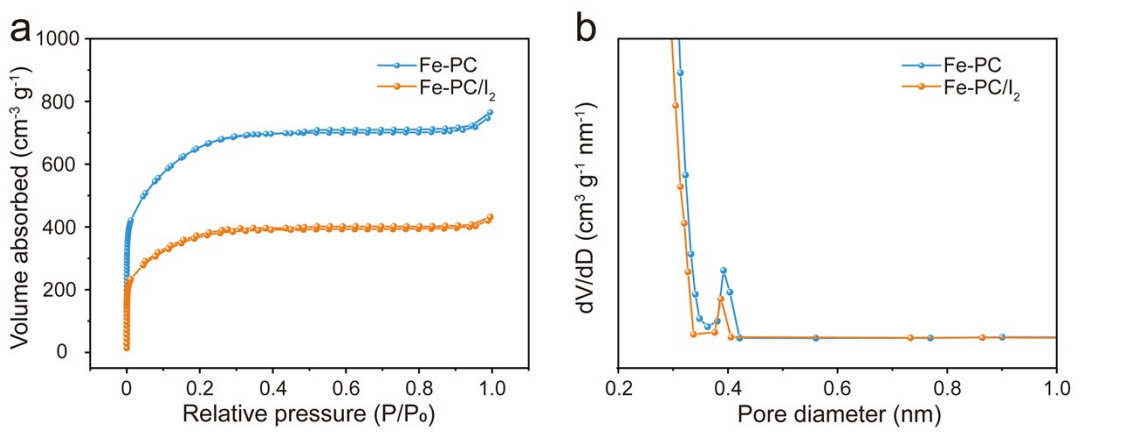

Figure S2. (a) Nitrogen adsorption and desorption isotherm of Fe-PC and Fe-PC/I_2. (b) Pore size distribution curves of Fe-PC and Fe-PC/I_2.

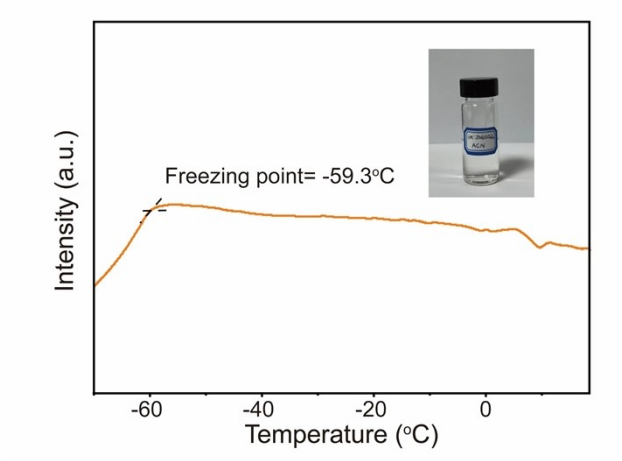

Figure S3. DSC curve of 1 M $Zn(ClO_4)_2$ in ACN.

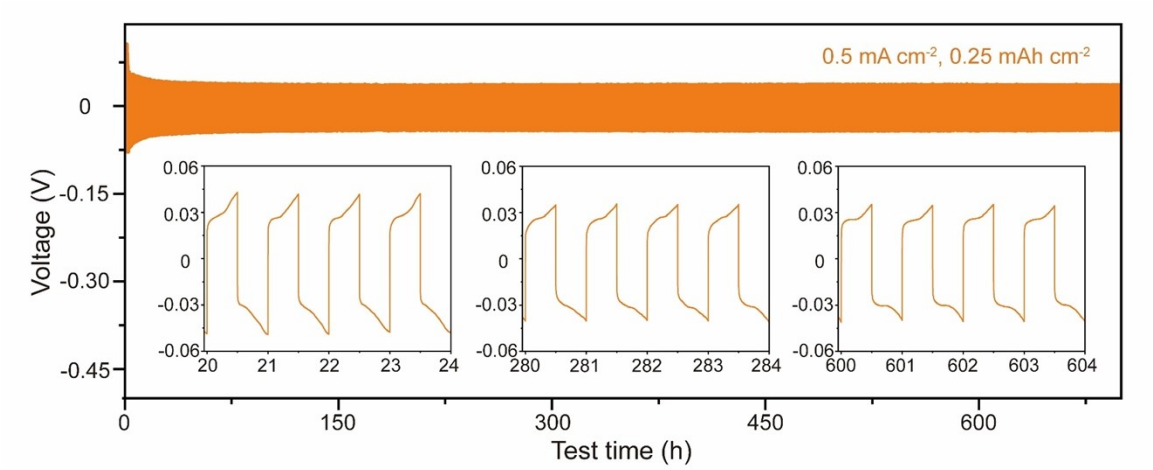

Figure S4. Cycling stability of Zn||Zn symmetrical cells in ACN-based electrolyte at 25 °C.

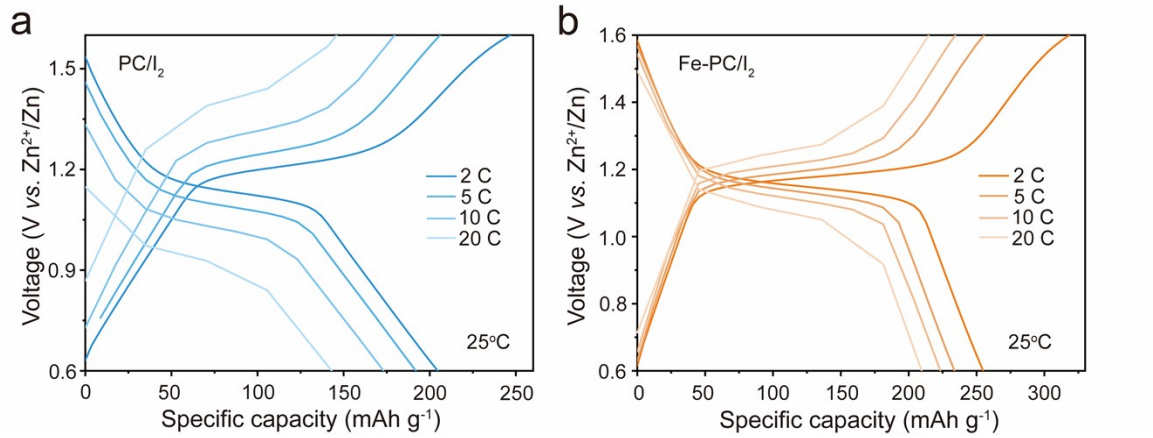

Figure S5. GCD curves of of PC/I_2 and $Fe\text{-}PC/I_2$ electrodes collected at different current densities at 25 ℃.

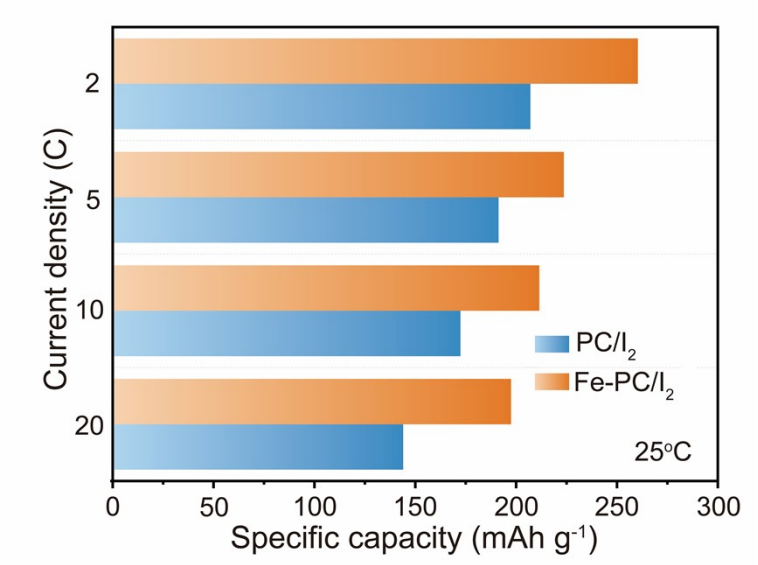

Figure S6. Rate performance of PC/I_2 and $Fe\text{-}PC/I_2$ electrodes at varying current densities and 25 °C.

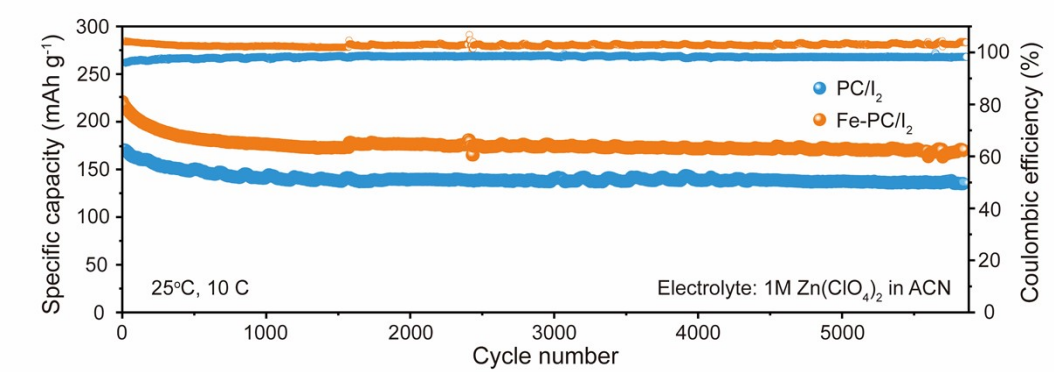

Figure S7. The cycling performance of PC/I_2 and $Fe\text{-}PC/I_2$ electrodes at 25°C and 10 C.

The higher diffusivity of the ACN–I_2 charge-transfer complexes at 25 °C partially compromises the immobilization effect of Fe single atoms, leading to a moderate capacity decay of approximately 40 mAh g^{-1} after 500 cycles while still sustaining stable cycling over 5800 cycles (Fig. S7).

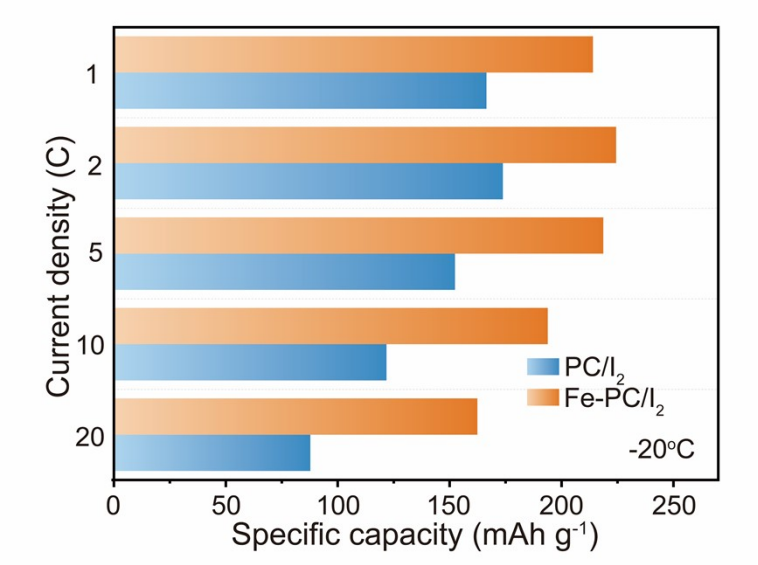

Figure S8. Rate performance of PC/I_2 and $Fe\text{-}PC/I_2$ electrodes at varying current densities and −20°C.

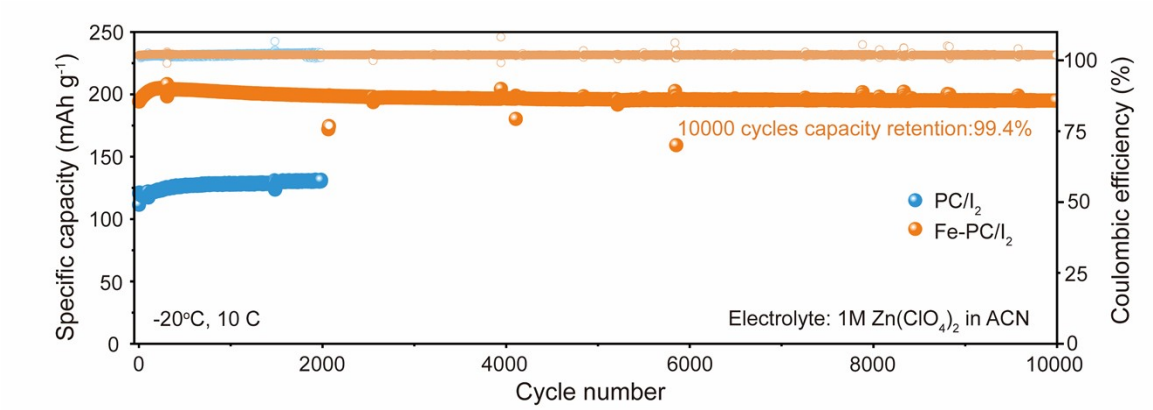

Figure S9. The cycling performance of PC/I_2 and $Fe\text{-}PC/I_2$ electrodes at −20°C and 10 C.

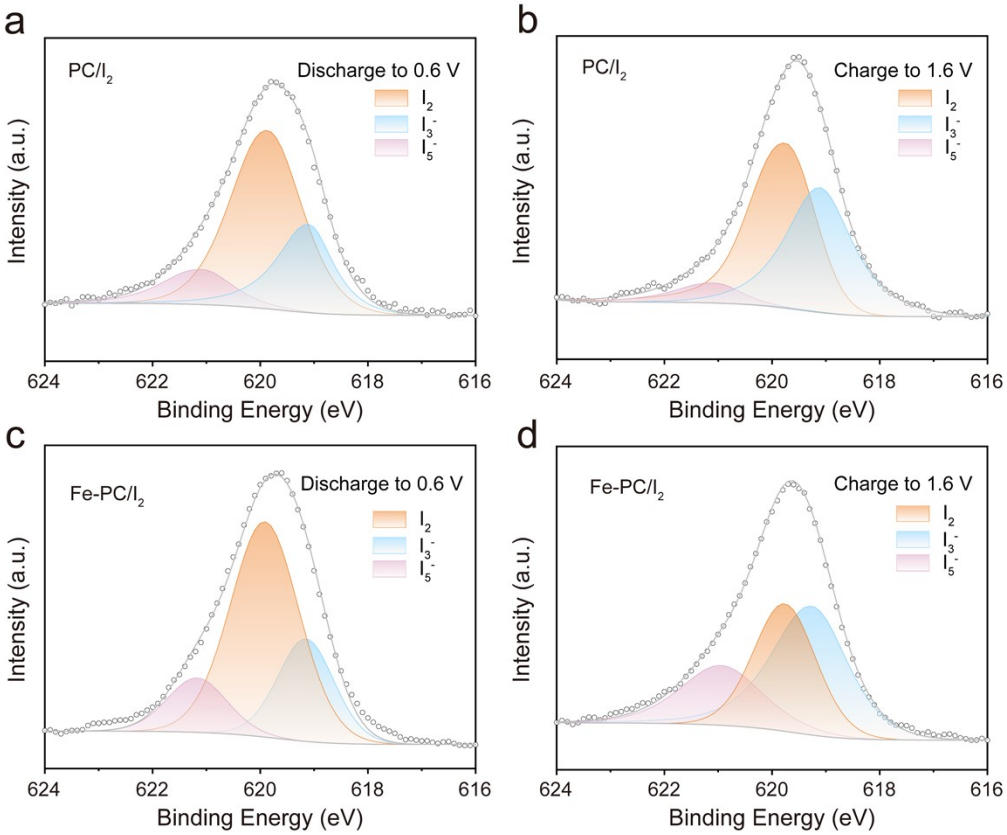

Figure S10. High-resolution I 3d XPS spectra of (a-b) PC/I_2 and (c-d) Fe-PC/I_2 electrodes at different charge/discharge states under −40°C.

The I 3d XPS spectra were deconvoluted into three peaks corresponding to I_3^- (619.2 eV), I_2 (619.8 eV), and I_5^- (621.1 eV) , which are in good agreement with recent works.[1-3] As shown in Fig. S10 (a) and (c), at the fully discharged state (0.6 V), characteristic peaks at 619.2, 619.8, and 621.1 eV are observed, which are assigned to I_3^-, I_2, and I_5^- species, respectively. Upon full charge to 1.6 V (Fig. S10 (b) and (d)), the Fe-PC/I_2 electrode exhibits a higher proportion of I_5^- and I_3^- species, whereas the PC/I_2 electrode primarily shows I_2 and a lower content of I_5^-. This distinct difference provides strong evidence that the iodine redox reaction on the Fe-PC/I_2 electrode proceeds via a liquid–liquid pathway.

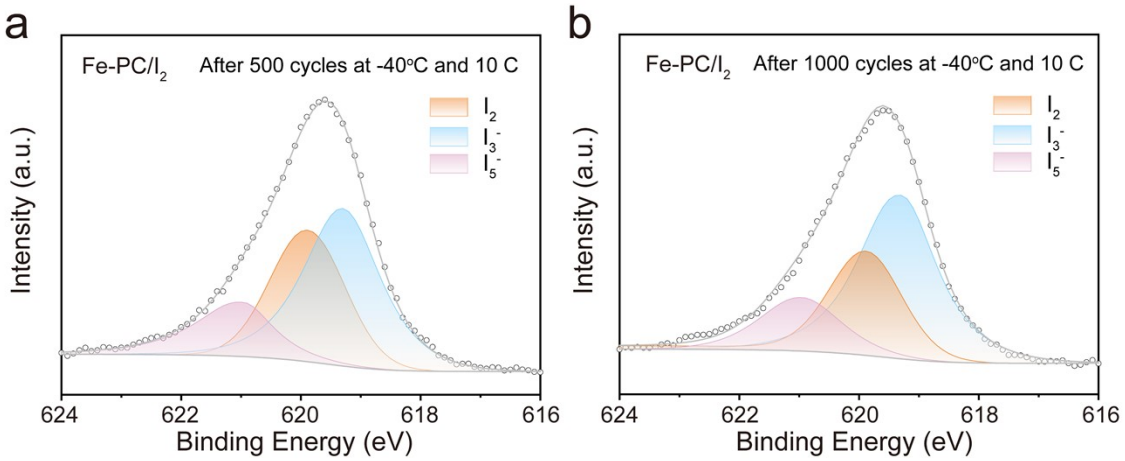

Fig. S11 I 3d XPS spectra of Fe-PC/I_2 electrode at 1.6 V: (a) after 500 cycles, (b) after 1000 cycles at −40°C and 10 C.

The I 3d XPS spectra of the electrodes for Fe-PC/I_2 after 500 and 1000 cycles were collected at 1.6 V to monitor the evolution of iodine species. After 500 and 1000 cycles (Fig. S11(a) and (b)), the characteristic peak of solid I_2 (619.8 eV) is markedly suppressed, while two prominent peaks emerge at 619.2 eV and 621.1 eV corresponding to I_3^- and I_5^- species, respectively. These results demonstrate that the Fe-PC electrode effectively confines the ACN-I_2 charge-transfer complex and suppresses the accumulation of solid iodine during prolonged cycling.

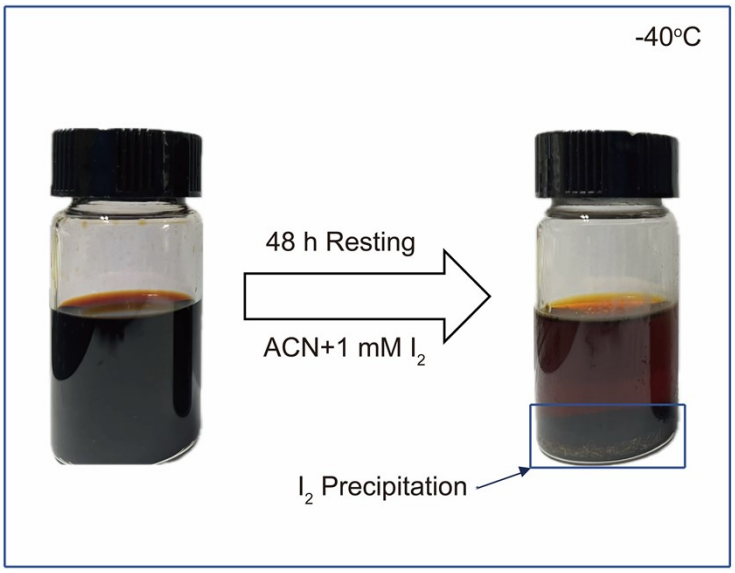

Figure S12. Visual dissolution experiment of iodine powder in ACN-based electrolyte (1 M $Zn(ClO_4)_2$ in ACN) at −40°C.

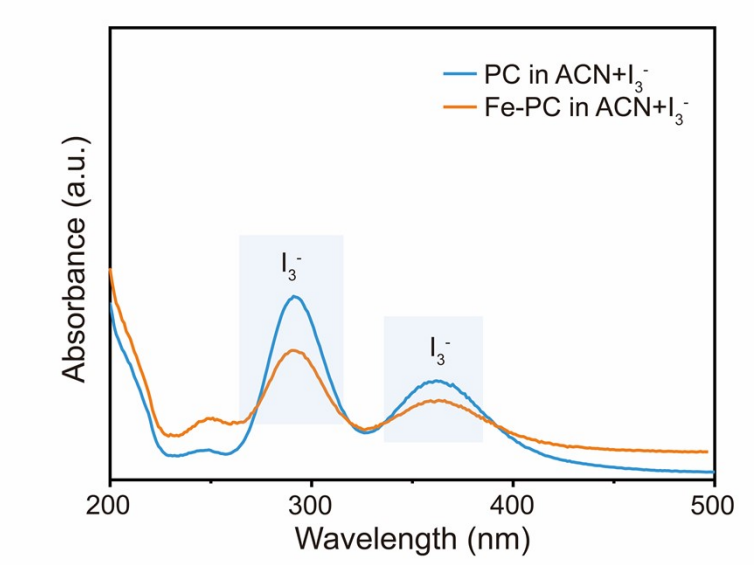

Figure S13. UV-vis spectra of the ACN-based electrolyte containing I_3^- (1 mM) after immersion with PC and Fe-PC.

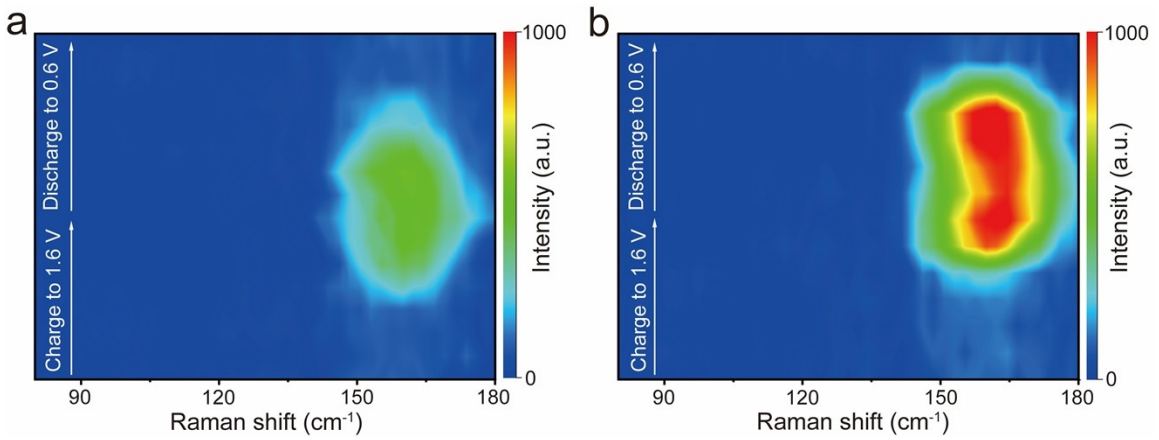

Figure S14. (a) In situ Raman spectroscopy of PC/I_2 at 25°C. (b) In situ Raman spectroscopy of Fe-PC/I_2 at 25°C.

The characteristic polyiodide (I_5^-) peak at 160 cm^{-1} for the Fe-PC/I_2 electrode progressively intensifies with increasing charge voltage and reversibly diminishes during discharge at 25°C (Fig. S14). This evolution reveals a sequential conversion of iodine species into high-order polyiodides at elevated charge voltages. Conversely, the persistently weak I_5^- signals observed for PC/I_2 electrode throughout the charge/discharge process indicate incomplete iodine conversion and inferior electrochemical reversibility.

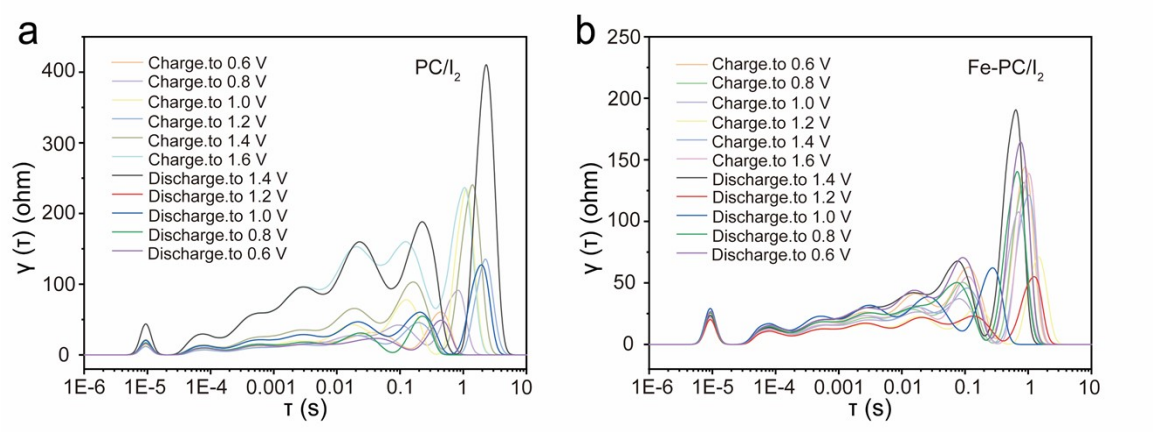

Figure S15. DRT analysis of (a) PC/I_2, (b) Fe-PC/I_2 at −40°C.

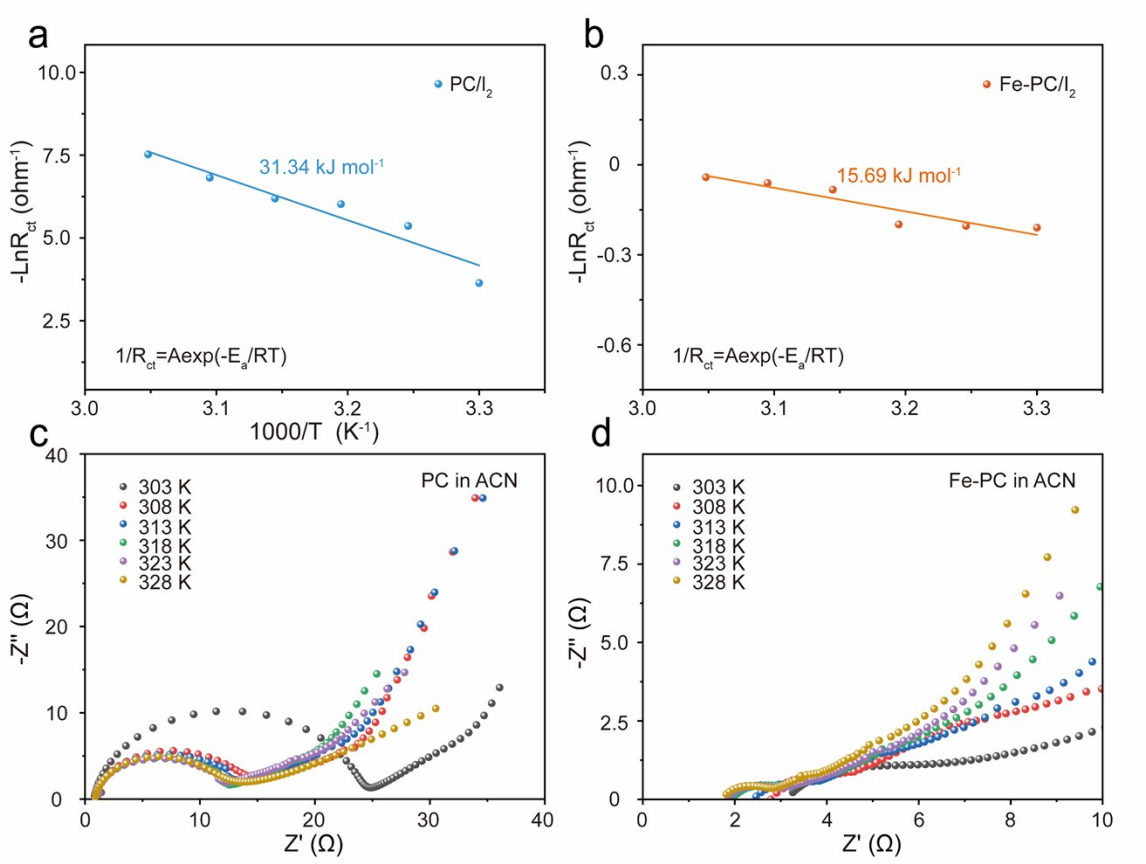

Figure S16. Arrhenius curves and comparison of activation energies of (a) PC/I_2, (b) Fe-PC/I_2 electrodes. EIS spectrums of (c) PC/I_2, (d) Fe-PC/I_2 at different temperatures.

References

1 T. Xiao, J.-L. Yang, R. J. Xu, H. Xu, H. Liu, J. Li, H. Bao, X. Jin, S.-J. Hwang, Z. Wang and H. J. Fan, *J. Am. Chem. Soc.*, 2025, **147**, 28820-28830.

2 X. Li, Y. Wang, Z. Chen, P. Li, G. Liang, Z. Huang, Q. Yang, A. Chen, H. Cui, B. Dong, H. He and C. Zhi, *Angew. Chem. Int. Edit.*, 2022, **61**, e202113576.

3 M. Li, W. Wang, Y. Liu, Q. Wang, T. Wang, X. He, Z. Zhou, H. Li, M. Zhou, K. Wang and K. Jiang, *Energy Environ. Mater.*, 2026, DOI: 10.1002/eem2.70236.